Article

Fatigue assessment of prestressed concrete slab-between-girder bridges

Eva O.L. Lantsoght[1,2,*], Rutger Koekkoek[3] , Cor van der Veen[4] and Henk Sliedrecht[5]

[1] Politécnico, Universidad San Francisco de Quito, Quito, Ecuador; elantsoght@usfq.edu.ec
[2] Concrete Structures, Delft University of Technology, Delft, the Netherlands; E.O.L.Lantsoght@tudelft.nl
[3] BAM Infraconsult, Gouda, the Netherlands; rutger.koekkoek@bam.com
[4] Concrete Structures, Delft University of Technology, Delft, the Netherlands; C.vanderveen@tudelft.nl
[5] Rijkswaterstaat, Ministry of Infrastructure and the Environment, Utrecht, the Netherlands; henk.sliedrecht@rws.nl
* Correspondence: elantsoght@usfq.edu.ec ; Tel.: (+593) 2 297-1700 ext. 1186

Received: date; Accepted: date; Published: date

Featured Application: The results of this work can be used for the evaluation of existing prestressed concrete slab-between-girder bridges for fatigue.

Abstract: In the Netherlands, the assessment of existing prestressed concrete slab-between-girder bridges showed that the thin, transversely prestressed slabs may be critical for static and fatigue punching when evaluated using the recently introduced Eurocodes. On the other hand, compressive membrane action increases the capacity of these slabs and changes the failure mode from bending to punching shear. To improve the assessment of the existing prestressed slab-between-girder bridges in the Netherlands, two 1:2 scale models of an existing bridge, the Van Brienenoord Bridge, were built in the laboratory and tested monotonically as well as under cycles of loading. The result of these experiments is: 1) the static strength of the decks, showing that compressive membrane action significantly enhances the punching capacity, and 2) the Wöhler curve of the decks, showing that compressive membrane action remains under fatigue loading. The experimental results can then be used for the assessment of the most critical existing slab-between-girder bridge. The outcome is that the bridge has sufficient punching capacity for static and fatigue loads, and thus that the existing slab-between-girder bridges in the Netherlands fulfil the code requirements for static and fatigue punching.

Keywords: Assessment; Bridge evaluation; Compressive membrane action; Concrete bridges; Fatigue; Fatigue assessment; Live loads; Prestressed concrete; Punching shear; Scale model.

---

1. Introduction

The majority of the bridges in the Dutch highway bridge stock were built in the decades following World War II, which was an era of rapid and extensive expansion of the Dutch road network. These bridges were designed for the live loads of that era, which resulted in lower demands on the bridges than the recently introduced Eurocode live loads from NEN-EN 1991-2:2003 [1]. In terms of capacity, the design capacities for shear and punching from the previously used Dutch codes (e.g. VBC 1995 – NEN 6723 [2]) are larger than those determined using the recently introduced Eurocode for concrete structures NEN-EN 1992-1-1:2005 [3]. With higher demands and lower capacities according to the Eurocodes, the outcome of an assessment is often that existing bridges do not fulfil the code requirements for brittle failure modes such as shear [4] and punching [5]. This problem is not limited to the Netherlands; similar discussions take place in Germany [6], Sweden [7], Switzerland [8], and other European countries, as well as in the United States [9], where bridge construction peaked in the 1930s (the New Deal) and between 1956 and 1992 (construction of the Interstate Highway System). As one can see, methods for an accurate assessment of existing bridges

Preprints (www.preprints.org) | NOT PEER-REVIEWED | Posted: 28 April 2019 doi:10.20944/preprints201904.0304.v1

are becoming increasingly important, as the safety of the traveling public should be protected, and at the same time, unnecessary bridge replacement or strengthening actions should be avoided [10].

The preliminary assessment of the existing bridges in the Netherlands according to the new Eurocodes was based on hand calculations (Quick Scans [11,12]), and categories of bridge types that require further study were identified. One such category contains prestressed slab-between-girder bridges. This subset contains about 70 bridges [5]. The structural system of these bridges is a combination of prestressed girders with the deck slab cast in between the girders and transversely prestressed. As a result, the top of the flange of the girders is flush with the top of the deck. Additionally, prestressed diaphragm beams provide stiffness to the overall system. Upon assessment, the thin deck slabs do not fulfil the code requirements for punching shear. One mechanisms that is not considered in the codes, but that enhances the capacity of these thin decks, is compressive membrane action [13-20]. Additionally, the fatigue capacity of the thin decks is subject to discussion, as it is not known if progressive cracking and damage accumulation affects the capacity-enhancing effect of compressive membrane action [21].

This work summarizes experimental results from testing 1:2 scale models of prestressed slab-between-girder bridges, and then applies these results to the punching and fatigue assessment of an existing bridge. We show how compressive membrane action improves the assessment for punching shear, and how the Wöhler curve from the fatigue tests can be used for the assessment of the bridge deck under fatigue. The summarized experiments are unique in nature, as the tested specimens give us insight in the behavior of slab-between-girder bridges as a structural system. Most fatigue testing in the past focused on testing small specimens [22,23] or structural elements [24-31] instead of structural systems. The insights from these experiments are now reported for the first time in the context of bridge assessment. This analysis shows that, based on the experimental evidence, it is found that the existing slab-between-girder bridges in the Netherlands fulfil the safety requirements of the code, and in particular the requirements for punching shear under static and fatigue live loading.

2. Materials and Methods

2.1. Description of case study bridge

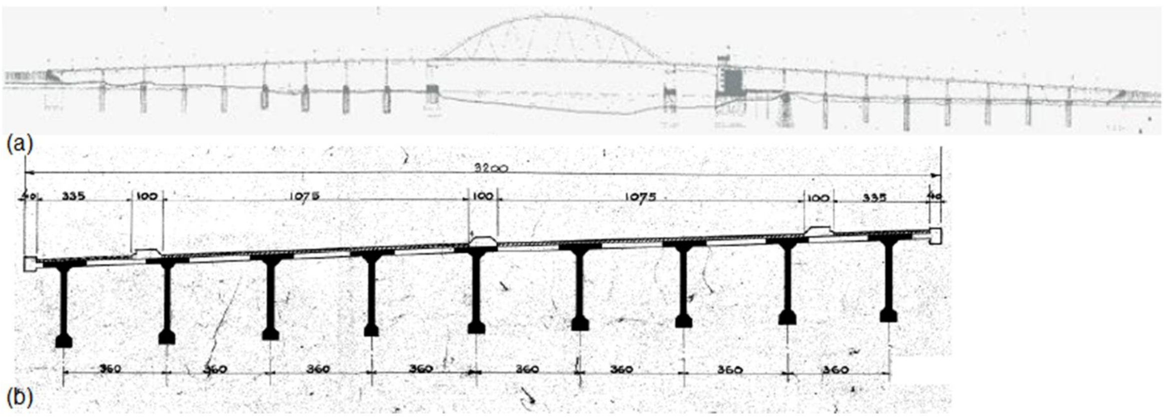

Figure 1. Van Brienenoord Bridge: (a) sketch of elevation of entire bridge structure, showing approach slabs as well as steel arch; (b) cross-section of the slab-between-girder approach bridge. Dimensions in cm.

Of the 70 slab-between-girder bridges in the Netherlands, the one that has the most critical slab geometry (largest span to depth ratio of 3.6 m / 0.2 m = 18) is the approach bridge of the Van Brienenoord Bridge in Rotterdam, see **Figure 1**a. The approach spans are 50 m in length and consist of thin, transversely post-tensioned decks cast in between simply supported post-tensioned girders, see **Figure 1**b [13]. The clear span of the slab is 2100 mm. The transverse prestressing level is 2.5 MPa. The duct spacing in the deck is 650 mm on center, and at some positions it is increased to 800 mm on center. **Table 1** gives the main properties of the geometry and reinforcement of the decks. Post-

Preprints (www.preprints.org) | NOT PEER-REVIEWED | Posted: 28 April 2019 doi:10.20944/preprints201904.0304.v1

tensioned crossbeams are built at the end of the spans and post-tensioned diaphragm beams are provided at 1/3 and 2/3 of the span length.

At the time of construction, the design concrete compressive strength of the deck was B35 ($f_{ck,cube}$ = 35 MPa) and of the girders B45 ($f_{ck,cube}$ = 45 MPa). Testing of cores taken from the deck slab resulted in an average $f_{cm,cube}$ = 98.8 MPa ($f_{ck,cube}$ = 84.6 MPa) as a result of the continued cement hydration. For the assessment calculations, it is conservatively assumed that the mean compressive cylinder strength f_{cm} = 65 MPa in the deck. The associated characteristic concrete compressive strength is f_{ck} = 53 MPa.

Table 1: Main properties of geometry and reinforcement of decks of Van Brienenoord Bridge.

Dimension	Value
Thickness h	200 mm
Concrete cover c	30 mm
Longitudinal reinforcement	ϕ8 mm – 250 mm
Effective depth longitudinal d_l	166 mm
Area of longitudinal reinforcement $A_{s,l}$	201.1 mm²/m
Longitudinal reinforcement ratio ρ_l	0.12%
Transverse reinforcement	ϕ8 mm – 200 mm
Effective depth transverse d_t	158 mm
Area of transverse reinforcement $A_{s,t}$	251.3 mm²/m
Transverse reinforcement ratio ρ_t	0.16%
Average effective depth d	162 mm
Average reinforcement ratio ρ_{avg}	0.14%
Prestressing reinforcement	462 mm² – 800 mm
Area of prestressing steel A_{sp}	0.5775 mm²/mm

2.2. Live load models

Two live load models are relevant for the assessment of the Van Brienenoord Bridge: Load Model 1 for the assessment of the punching capacity, and Fatigue Load Model 1 for the fatigue assessment, both from NEN-EN 1991-2:2003 [1].

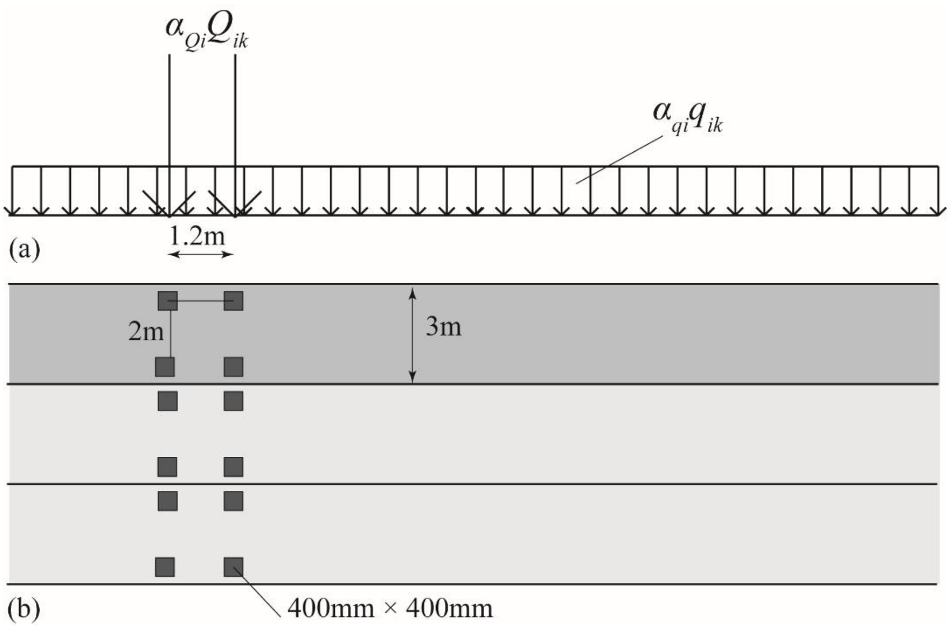

Figure 2. Live Load Model 1 from NEN-EN 1991-2:2003 [1]: (a) elevation; (b) top view. Edited from [12], reprinted with permission.

Preprints (www.preprints.org) | NOT PEER-REVIEWED | Posted: 28 April 2019 doi:10.20944/preprints201904.0304.v1

Live Load Model 1 combines a distributed lane load with a design tandem. The design tandem has the following characteristics: 1) wheel print of 400 mm × 400 mm, 2) axle distance of 1.2 m, and 3) transverse spacing between wheels of 2 m. The magnitude of the axle load is α_{Q1} × 300 kN in the first lane, α_{Q2} × 200 kN in the second lane, and α_{Q3} × 300 kN in the third lane [12]. For the Netherlands, the values of all α_{Qi} = 1 with i = 1…3. The uniformly distributed load acts over the full width of the notional lane of 3 m wide, and equals α_{q1} × 9 kN/m² for the first lane, and α_{qi} × 2.5 kN/m² for all other lanes. For bridges with three or more notional lanes in the Netherlands, the value of α_{q1} = 1.15 and α_{qi} = 1.4 with i > 1. **Figure 2** shows a sketch of live Load Model 1.

Fatigue Load Model 1 has the same configuration as Load Model 1, with 0.7Q_{ik} for the axle loads and 0.3q_{ik} for the distributed lane loads. In other words, the axle load becomes 0.7 × 300 kN = 210 kN, and the load per wheel print becomes 105 kN. The distributed lane load is 0.3 × 1.15 × 9 kN/m² = 3.105 kN/m². The fatigue load model has as a reference load 2 million trucks per year. In the Netherlands, the guidelines for the assessment of bridges (RBK [32]) use a higher number of passages: 2.5 million trucks per year. Over a lifespan of 100 years, the result is 250 million truck passages.

In the Netherlands, assessment is carried out both with a wheel print of 400 mm × 400 mm (as prescribed by the Eurocode 1 NEN-EN 1991-2:2003 [1]) and of 230 mm × 300 mm (used for the fatigue evaluation of joints, but often used as an additional check in assessment as well).

2.3. Description of experiments

Two 1:2 scale models of an existing bridge were built in the laboratory and tested monotonically as well as under cycles of loading. Full descriptions of the first series of static tests [5,13], first series of fatigue tests [33-35], and second series of fatigue tests [36,37] can be found elsewhere. The description in this paper is limited to the information necessary for interpreting the test results for the application to assessment of the case study bridge.

The first 1:2 scale model (6.4 m × 12 m, see **Figure 3**) used four prestressed concrete T-girders with a center-to-center spacing of 1.8 m, length l = 10.95 m, and height h = 1.3 m; two post-tensioned crossbeams (b = 350 mm, h = 810 mm), and three transversely post-tensioned decks with h = 100 mm and b = 1050 mm between the girders. The post-tensioning of the deck was applied through prestressing bars placed in 30 ducts of diameter 40 mm, spaced 400 mm apart. To increase the number of experiments that could be carried out on this scale model, the middle deck was removed after testing and a new deck was cast. One segment of the new deck contained ducts of diameter 30 mm, spaced 300 mm apart to study the influence of the duct spacing.

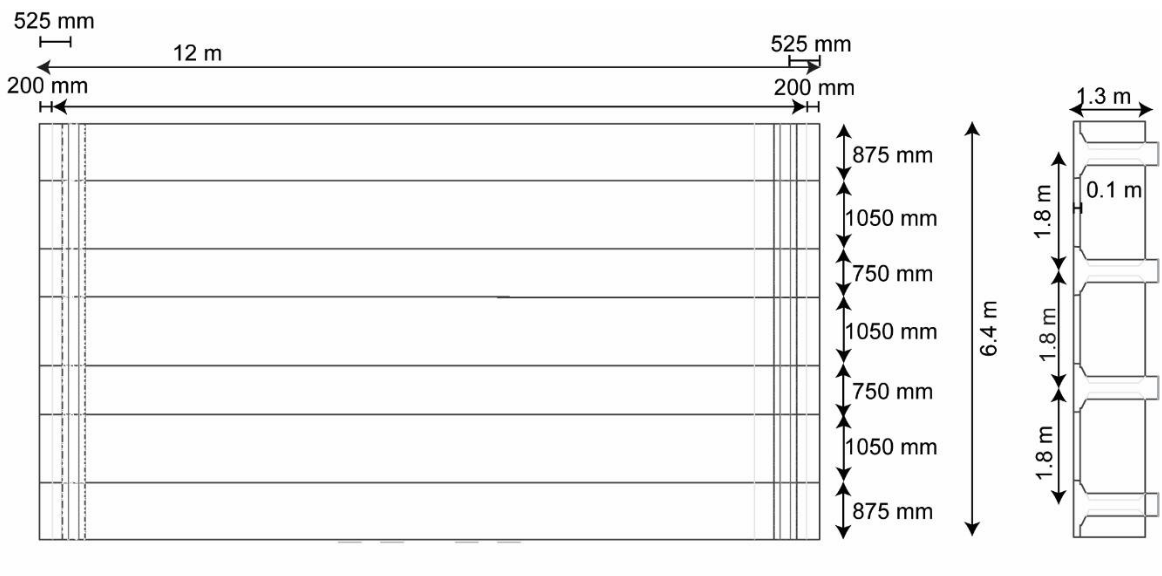

(a) (b)

Figure 3. Dimensions of first 1:2 scale model: (a) top view; (b) cross-section view. Figure adapted from [34]. This figure was originally published in Vol. 116 of the ACI Structural Journal.

The second 1:2 scale model (4.6 m × 12 m, see **Figure 4**) used three prestressed concrete bulb T-girders and two post-tensioned decks. The dimensions of the girders, crossbeams, and decks are the same as for the first 1:2 scale model, with the exception of the shape of the girders (T-girders in the first scale model and bulb T-girders in the second scale model). For the second scale model, the top flange of the girders was cast in the laboratory, monolithically with the deck. The advantage of this approach is that the weight of the girders is reduced, which facilitates transportation and handling.

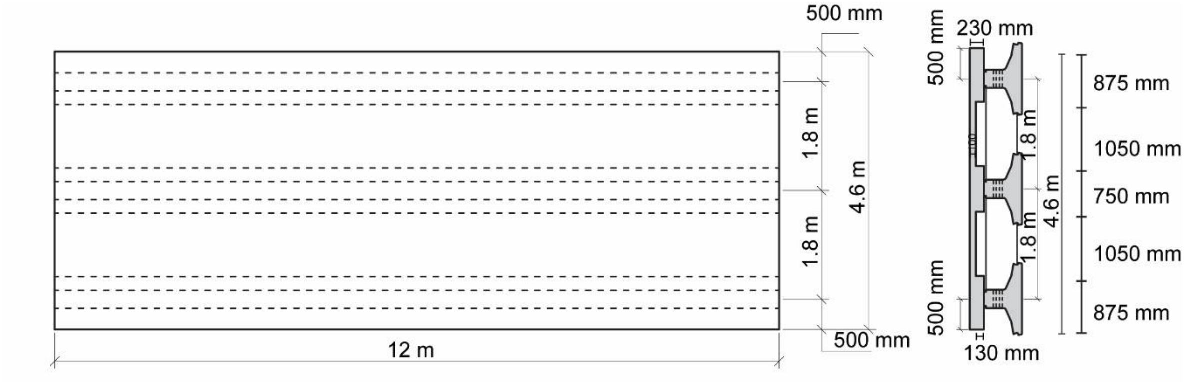

(a) (b)

Figure 4. Overview of second 1:2 scale setup: (a) top view; (b) cross-section view. Figure adapted from [37]. This figure was originally published in Vol. 116 of the ACI Structural Journal.

Standard cube specimens are used for determining the concrete compressive strength for the concrete of the different casts. The results for the 28 days strength are as follows: $f_{cm,cube}$ = 75 MPa for the original slab in setup 1, $f_{cm,cube}$ = 68 MPa for the newly cast slab in setup 1, $f_{cm,cube}$ = 81 MPa for the first cast of setup 2, and $f_{cm,cube}$ = 79 MPa for the second cast of setup 2.

Mild steel reinforcement is used for the longitudinal and transverse reinforcement in the deck slabs. In setup 1, the longitudinal reinforcement is ϕ = 6 mm at 200 mm o.c. top and bottom, and the transverse reinforcement is ϕ = 6 mm at 250 mm o.c. top and bottom. In setup 2, the longitudinal reinforcement is ϕ = 8 mm at 200 mm o.c. top and bottom, and the transverse reinforcement is ϕ = 8 mm at 240 mm o.c. top and bottom. The clear cover to the reinforcement is 7 mm. The mild steel reinforcement in the setups is B500B steel, except for the bars of 6 mm diameter, for which B500A steel was used. Stress-strain curves of the mild steel for all bar diameter are measured in the laboratory, see [33,36].

The prestressing steel in the girders is Y1860S tendons and the prestressing steel in the crossbeams and slabs is Y1100H prestressing bars with a diameter of 15 mm. The transverse prestressing in the deck results in an axial compressive stress of 2.5 MPa.

The size of the concentrated load in the experiments is 200 mm × 200 mm for the experiments on the original first setup, which is 1:2 scale of the wheel print of 400 mm × 400 mm from the design tandem of Load Model 1 in NEN-EN 1991-2:2003 [1]. For all other experiments, the size of the loading plate was 115 mm × 150 mm, or 1:2 scale the wheel print of 230 mm × 300 mm used for the assessment in the Netherlands of bridge joints for fatigue.

The load is applied with a hydraulic jack mounted in a steel frame test setup. For the static tests, the load is applied with a stepwise monotonic loading protocol. In two experiments, a loading protocol with three cycles per load levels is used. For the static tests and the tests with three cycles per load level, the load is applied in a displacement-controlled way. For the fatigue tests, the load is cycled between a lower limit and upper limit, with the lower limit 10% of the upper limit. A sine function is used with a frequency of 1 Hz. The load is applied in a force-controlled way for the fatigue tests. If fatigue failure does not occur after a large number of cycles, the upper load level is increased (and the associated lower limit of 10% of the upper limit adjusted as well) and fatigue testing is continued.

3. Results

3.1. Results of experiments

The complete results of all experiments can be consulted in [5] for the static tests on the first setup, in [34] for the fatigue tests on the first setup, and in [37] for the tests on the second setup. Here, only the results that are relevant for the assessment of the case study bridge are summarized.

Table 2 gives an overview of the relevant static tests from the first setup (BB tests) and second setup (FAT tests). For the BB series, all experiments are numbered consecutively. For the FAT series, the test number gives information about the experiment: FAT (fatigue testing series of experiments on setup 2), followed by the test number, and then S (static test) or D (dynamic test), and 1 (load applied through one loading plate representing a single wheel load) or 2 (load applied through two loading plates representing a double wheel load). The tables gives the size of the loading plate used for testing, the load at failure P_{max}, the age of the concrete of the slab at the moment of testing, and the concrete cube compressive strength $f_{cm,cube}$ determined at the day of testing the slab.

Table 2. Overview of static tests used for assessment of case study bridge

Test number	Size load (mm × mm)	P_{max} (kN)	Age (days)	$f_{cm,cube}$ (MPa)
BB1	200 × 200	348.7	96	80.0
BB2	200 × 200	321.4	99	79.7
BB7	200 × 200	345.9	127	80.8
BB19	200 × 200	317.8	223	79.9
FAT1S1	150 × 115	347.8	94	82.2
FAT7S1	150 × 115	393.7	240	88.8
FAT8S2	2 of 150 × 115	646.1	245	88.6

Table 3 gives an overview of the fatigue tests. Here, all tests are considered relevant for the fatigue assessment, since all fatigue tests are used to derive the Wöhler curves. The test number is given, with BB the experiments on the first setup and FAT the experiments on the second setup. Then, the number of the setup is listed, with "1, new" for the experiments that were carried out on the newly cast deck in the first setup. Next, the size of the loading plate used for applying the load on the slab is reported, followed by "Wheel", which can be S (single wheel print) or D (double wheel print). Then, the upper load level used in the test, F/P_{max} (with P_{max} from a static test) is given, as well as N, the number of cycles. For the variable amplitude fatigue tests, N is the number of cycles for the associated load level F/P_{max}. After N cycles at load level F/P_{max}, given on one row of **Table 3**, the test is continued with N cycles at another load level F/P_{max}, given on the next row. The column "Age" gives the age of the slab at the age of testing, and $f_{cm,cube}$ gives the associated cube concrete compressive strength. For fatigue tests that lasted several days, a range of ages is given in the column "Age", indicating the age of the concrete in the slab at the beginning of testing and at the end of testing. Similarly, a range of compressive strengths is given for $f_{cm,cube}$, representing the strength determined at the beginning and end of testing.

Table 3. Overview of punching fatigue experiments

Test Number	Setup	Size load (mm × mm)	Wheel	F/P_{max}	N	Age (days)	$f_{cm,cube}$ (MPa)
BB17	1	200 × 200	S	0.80	13	147	82.6
BB18	1	200 × 200	S	0.85	16	56	82.6
BB23	1	200 × 200	S	0.60	24,800	301	79.9
BB24	1	200 × 200	S	0.45	1,500,000	307-326	79.9
BB26	1, new	150 × 115	S	0.48	1,405,337	35-59	70.5-76.7
BB28	1, new	150 × 115	S	0.48	1,500,000	68-97	76.8-77.1

 doi:10.20944/preprints201904.0304.v1

				0.58	1,000,000	97-113	77.1-77.3
				0.70	7144	113	77.3
BB29	1, new	150 × 115	S	0.58	1,500,000	117-136	77.3-77.5
				0.64	264,840	136-139	77.5-77.6
BB30	1, new	150 × 115	D	0.58	100,000	143-144	77.6
				0.50	1,400,000	144-162	77.6-77.8
				0.58	750,000	162-171	77.8-77.9
				0.67	500,000	171-177	77.9-78.0
				0.75	32,643	177	78.0
BB32	1, new	150 × 115	S	0.70	10,000	184	78.1
				0.58	272,548	185-187	78.1
FAT2D1	2	150 × 115	S	0.69	100,000	102-144	82.6-84.6
				0.58	2,915,123		
				0.69	100,000		
				0.75	150,000		
				0.81	20,094		
FAT3D1	2	150 × 115	S	0.69	200,000	149-168	84.9-85.8
				0.58	1,000,000		
				0.69	100,000		
				0.75	300,000		
				0.81	6114		
FAT4D1	2	150 × 115	S	0.58	1,000,000	169-190	85.8-86.8
				0.69	200,000		
				0.75	100,000		
				0.81	63,473		
FAT5D1	2	150 × 115	S	0.71	10,000	192-217	91.6-89.6
				0.51	1,000,000		
				0.61	100,000		
				0.66	1,000,000		
				0.71	1424		
FAT6D1	2	150 × 115	S	0.71	10,000	219-239	89.6-88.8
				0.51	1,000,000		
				0.61	100,000		
				0.71	160,000		
				0.51	410,000		
				0.71	26,865		
FAT9D2	2	150 × 115	D	0.59	500,000	246-255	88.5-88.2
				0.65	209,800		
FAT10D2	2	150 × 115	D	0.63	100,000	260-284	90.2-91.3
				0.56	1,000,000		
				0.63	950,928		
FAT11D2	2	150 × 115	D	0.67	100,000	288-315	91.5-92.8
				0.60	1,000,000		
				0.67	1,100,000		
				0.75	1720		
FAT12D1	2	150 × 115	S	0.89	30	318	85.9
FAT13D1	2	150 × 115	S	0.86	38	319	85.8

3.2. Resulting Wöhler curve

To find the Wöhler curve of the fatigue experiments, the relation between the logarithm of the number of cycles N and the applied load ratio F/P_{max} is plotted, see **Figure 5**. The variable amplitude loading tests are interpreted as follows for this curve: if N_1 cycles at load level F_1 are applied, followed

Preprints (www.preprints.org) | NOT PEER-REVIEWED | Posted: 28 April 2019 doi:10.20944/preprints201904.0304.v1

by N_2 cycles at F_2, and then N_3 cycles to failure at F_3, with increasing load levels $F_1 < F_2 < F_3$, it is then conservative to assume that the slab can withstand $N_1 + N_2 + N_3$ cycles at load level F_1, $N_2 + N_3$ cycles at load level F_2, and N_3 cycles at load level F_3. This approach leads to three datapoints for one variable amplitude fatigue test. As a result of this approach, we obtained 16 datapoints on the first setup and 28 datapoints on the second setup, resulting in the 44 datapoints in **Figure 5**. The average value of the Wöhler curve is shown as "Mean" in **Figure 5** and is described with the following expression, using S for the load ratio and N for the number of cycles to failure:

$$S = -0.062 \log N + 0.969 \quad (1)$$

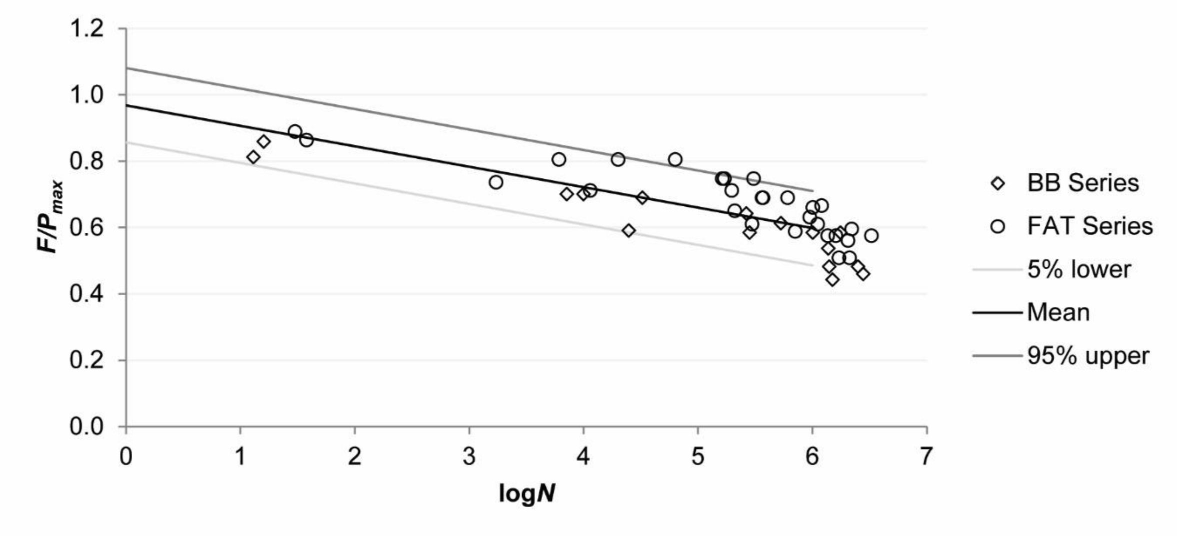

Figure 5. Relation between number of cycles N and applied load ratio F/P_{max} in all fatigue experiments, from [37]. Reprinted with permission. This figure was originally published in Vol. 116 of the ACI Structural Journal.

Since the assessment will be carried out separately for one and two wheel prints, it is interesting to look at the difference in Wöhler curve for the experiments with one and two wheel prints. **Figure 6** gives these results, with the datapoints from the FAT series for a single wheel print in **Figure 6**a and the datapoints for a double wheel print in **Figure 6**b. The markers in **Figure 6** are different for the datapoints obtained at a number of cycles that results in failure and a number of cycles that was calculated with the conservative assumption mentioned previously. The Wöhler curve for the datapoints with a single wheel load is:

$$S = -0.066 \log N + 1.026 \quad (2)$$

The 5% lower bound (characteristic value) of this expression, which can be used for assessment, is:

$$S_{char} = -0.066 \log N + 0.922 \quad (3)$$

The Wöhler curve for the datapoints with a double wheel load is:

$$S = -0.045 \log N + 0.885 \quad (4)$$

The 5% lower bound of this expression is:

$$S_{char} = -0.045 \log N + 0.825 \quad (5)$$

The slope of the Wöhler curve for the case with two wheel loads is lower than for the case with a single wheel load. However, for the case with a double wheel load, no low-cycle fatigue experimental results are available. For one load cycle Eq. (2) gives a load ratio of 1.026 and for Eq. (4) this value is 0.885. The difference between the two Wöhler curves for one cycle is significant. However, for 1 million load cycles, Eq. (2) gives a load ratio of 0.63 and Eq. (4) a load ratio of 0.62. For a large number

Preprints (www.preprints.org) | NOT PEER-REVIEWED | Posted: 28 April 2019 doi:10.20944/preprints201904.0304.v1

of load cycles, the difference between the two Wöhler curves thus becomes smaller. It is the large number of cycles that need to be considered for the assessment of existing bridges.

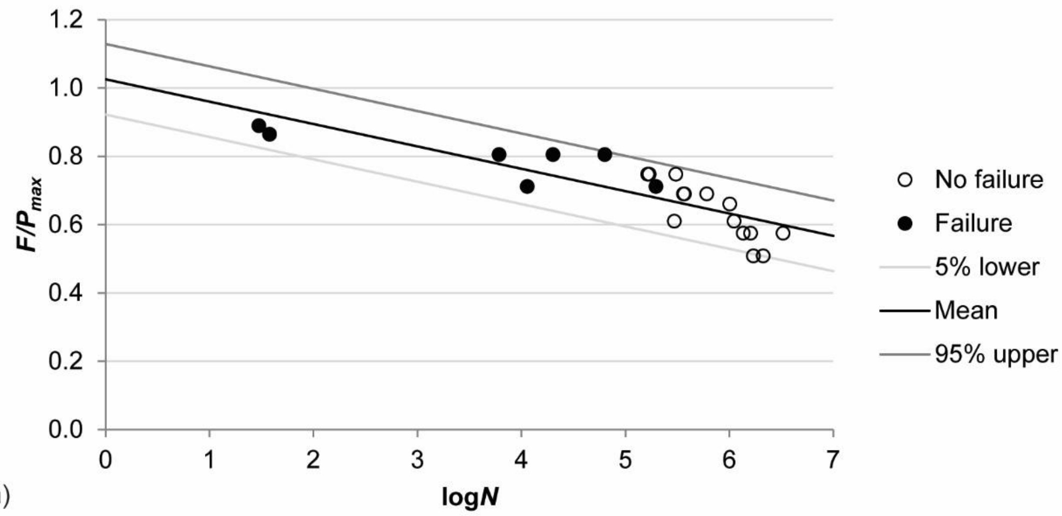

(a)

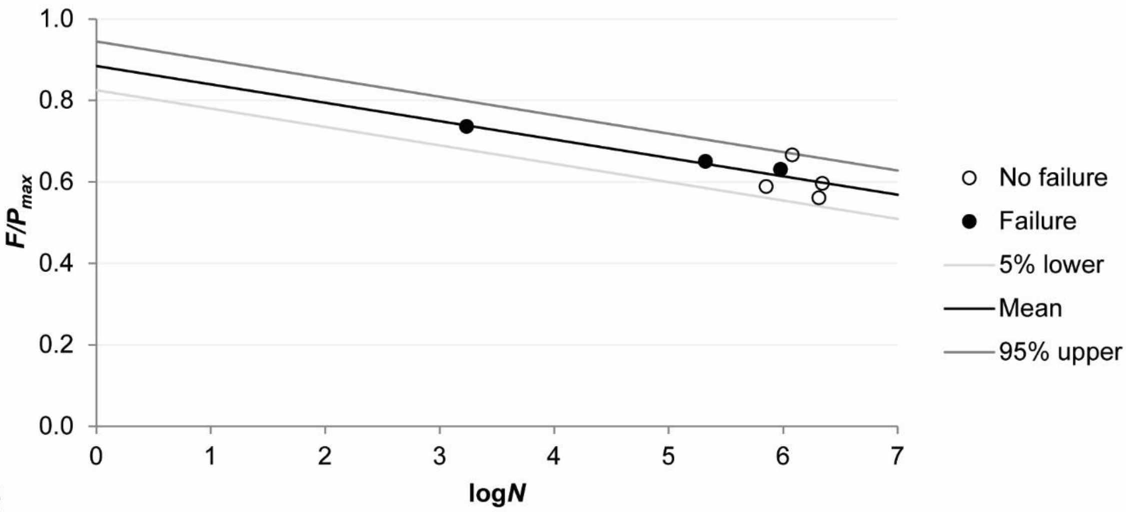

(b)

Figure 6. Relation between number of cycles N and applied load level F/P_{max} for (a) a single wheel load; and (b) a double wheel load, from [37]. Reprinted with permission. This figure was originally published in Vol. 116 of the ACI Structural Journal.

3.3. Assessment of case study bridge for punching

First, the capacity of the thin slab for punching is evaluated based on the experimental results. The shear capacity according to NEN-EN 1992-1-1:2005 [3] is calculated:

$$v_{Rd,c} = C_{Rd,c} k \left(100 \rho_{avg} f_{ck}\right)^{1/3} + k_1 \sigma_{cp} \geq v_{\min} + k_1 \sigma_{cp} \tag{6}$$

with

$$k = 1 + \sqrt{\frac{200\text{mm}}{d}} \leq 2 \tag{7}$$

and

$$\rho_{avg} = \sqrt{\rho_l \times \rho_t} \tag{8}$$

$$\sigma_{cp} = \frac{\sigma_{cx} + \sigma_{cy}}{2} \tag{9}$$

Preprints (www.preprints.org) | NOT PEER-REVIEWED | Posted: 28 April 2019 doi:10.20944/preprints201904.0304.v1

The recommended value for $k_1 = 0.1$, for $C_{Rd,c} = 0.18/\gamma_c$ with $\gamma_c = 1.5$ and for v_{min}:

$$v_{\min} = 0.035k^{3/2}\sqrt{f_{ck}} \tag{10}$$

Using the properties in **Table 1**, we find that $k = 2$ and the punching shear stress capacity of the case study bridge equals:

$$v_{Rd,c} = \frac{0.18}{1.5}\times 2\times\left(100\times 0.001388\times 53.3\text{MPa}\right)^{1/3} + 0.1\times 1.25\text{MPa} = 0.572\text{MPa} \tag{11}$$

To find the maximum punching force, we calculate the punching perimeter around the 400 mm wheel print as sketched in Figure 7:

$$u = 4\times 400\text{mm} + 2\pi\times 2\times 162\,\text{mm} = 3636\text{mm} \tag{12}$$

For the 230 mm × 300 mm wheel print, the punching perimeter length becomes:

$$u = 2\times\left(230\text{mm} + 300\text{mm}\right) + 2\pi\times 2\times 162\text{mm} = 3096\text{mm} \tag{13}$$

The maximum punching force for these two wheel prints then becomes:

$$V_{Rd,c} = 0.572\text{MPa}\times 3636\text{mm}\times 162\text{mm} = 336.8\text{kN} \tag{14}$$

$$V_{Rd,c} = 0.572\text{MPa}\times 3096\text{mm}\times 162\text{mm} = 286.8\text{kN} \tag{15}$$

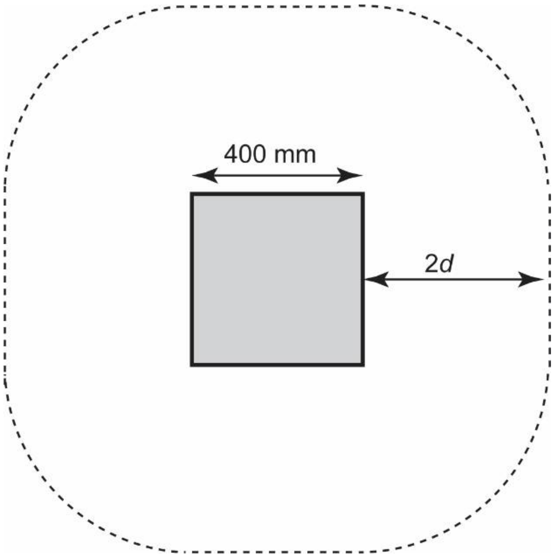

Figure 7. Punching perimeter around wheel print

The load that the deck has to resist is a combination of the concentrated live load and distributed live load. The axle load of 300 kN results in a wheel load of 150 kN. The distributed lane load is 1.15 × 9 kN/m² = 10.35 kN/m². The contributions of the self-weight and asphalt are respectively 25 kN/m³ × 200 mm = 5 kN/m² and 23 kN/m³ × 120 mm = 2.8 kN/m². The area over which these loads are considered is the area within the punching perimeter, A_u = (400mm)² + 4 × 162mm × 400mm + π(162mm/2)² = 439,812 mm² = 0.4398 m². The corresponding loads for the distributed lane load, self-weight, and asphalt then become 4.55 kN, 2.2 kN, and 1.23 kN when the Eurocode wheel print is considered. For the smaller wheel print, the area within the punching perimeter becomes A_u = 0.2613 m², resulting in loads of 2.7 kN, 1.3 kN, and 0.7 kN respectively for the distributed lane load, the self-weight, and the asphalt.

The load combination for the assessment of existing bridges in the Netherlands depends on the required safety level, as prescribed by NEN 8700:2011 [38] and the RBK (Guidelines for the Assessment of Existing Bridges) [32]. The highest level is the "Design" level (associated reliability index $\beta = 4.3$), which gives the following load combination: $U = 1.25DL + 1.25DW + 1.50LL$, with DL

the dead load, *DW* the superimposed dead load, and *LL* the live load. The resulting factored concentrated load for evaluation then becomes 236 kN for the 400 mm × 400 mm wheel print and 232 kN for the 230 mm × 300 mm wheel print.

The assessment is carried out based on the Unity Check. The Unity Check is the ratio of design demand to design capacity; for punching in this case, the Unity Check is the ratio of the factored concentrated load acting on the wheel print to the design punching shear force capacity. To fulfil the code requirements, the Unity Check has to be smaller than 1. **Table 4** gives an overview of the resulting Unity Checks for the different wheel prints studied. It can be seen that assessing the deck with the Eurocode already fulfils the requirements. In the introduction, we stated that there is discussion about the punching capacity of the decks in the existing slab-between-girder bridges. The reason why this assessment already shows that the deck fulfils the code requirements is the higher punching capacity that is found based on the results of drilled cores.

Table 4. Overview of resulting Unity Check according to Eurocode

Wheel print	V_{Ed} (kN)	$V_{Rd,c}$ (kN)	Unity Check
400 mm × 400 mm	236	337	0.70
230 mm × 300 mm	232	287	0.81

In a next step of the assessment, the maximum loads obtained in the static tests are applied to the assessment of the Van Brienenoord Bridge. When assessing the bridge based on the results of the experiments, we can replace the design capacity according to the Eurocode $V_{Rd,c}$ with the capacity obtained in the tests. To translate the capacity obtained in the test to a representative design capacity of the case study bridge, we have to consider the following (see Annex D of NEN-EN 1990:2002 [39]):

- the laboratory setup is 1:2 scale of the case study bridge, resulting in a factor 2^2;
- considering scaling laws, a scale factor of 1.2 [13] has to be included on the capacity;
- the partial factor derived from the experiments γ_T has to be included.

First, we will derive the partial factor from the experiments γ_T. To calculate this factor, we compare the punching capacity obtained in the static experiments with the average punching stress capacity $v_{R,c}$ according to NEN-EN 1992-1-1:2005 [3]. The expression for $v_{R,c}$ is given in the background report of Eurocode 2 [40] as follows:

$$v_{R,c} = 0.18 \times k \times \left(100 \times \rho_{avg} \times f_{cm}\right)^{1/3} + 0.08\sigma_{cp} \tag{16}$$

To find the punching shear capacity $V_{R,c}$ the stress $v_{R,c}$ is then multiplied with $u \times d$, with u determined as in **Figure 7** for the considered wheel print. **Table 5** then combines the experimental results V_{exp} and the predicted capacities $V_{R,c}$, as well as the ratio of tested to predicted capacity $V_{exp}/V_{R,c}$. The average value of $V_{exp}/V_{R,c}$ is 2.61, with a standard deviation of 0.296 and coefficient of variation of 11%. This information then leads to the derivation of γ_T as determined in Annex C of NEN-EN 1990:2002 [39]:

$$\gamma_T = \frac{\mu}{B_{Rd}} \tag{17}$$

with

$$B_{Rd} = \mu\left(1 - \alpha \times \beta \times COV\right) = 2.61\left(1 - 0.8 \times 4.3 \times 0.11\right) = 1.622 \tag{18}$$

with $\alpha = 0.8$ the factor for considering experimental results and β the target reliability index. The value for γ_T then becomes:

$$\gamma_T = \frac{\mu}{B_{Rd}} = \frac{2.61}{1.622} = 1.61 \tag{19}$$

As for the influence of the difference in scale between the test setup in the laboratory and the case study bridge, the experimental result V_{exp} can be scaled to the capacity of the bridge V_{BB} as follows:

Preprints (www.preprints.org) | NOT PEER-REVIEWED | Posted: 28 April 2019 doi:10.20944/preprints201904.0304.v1

$$V_{BB} = V_{exp} \times \frac{2^2}{1.2} \tag{20}$$

where the factor 2^2 corrects for the 1:2 scale and 1.2 is the scaling factor. The design capacity based on the test results is then:

$$V_{BB,d} = \frac{V_{BB}}{\gamma_T} \tag{21}$$

Table 6 shows the results for V_{BB} according to Eq. (20) and $V_{BB,d}$ according to Eq. (21), as well as the demand V_{Ed} that corresponds to the wheel print in the experiment under consideration (see **Table 4**). The average value of $V_{BB,d}/V_{Ed}$ = 3.06, which means that the margin of safety is 3.23, or that the Unity Check is the inverse, UC = 0.33. When comparing this value based on the experiments to the values in **Table 4**, we can observe the beneficial effect of compressive membrane action on the capacity of thin transversely prestressed concrete slabs.

Table 5. Comparison between mean predicted punching capacity and punching capacity in experiment.

Test number	Wheel print (mm × mm)	V_{exp} (kN)	$V_{R,c}$ (kN)	$V_{exp}/V_{R,c}$
BB1	200 × 200	348.7	141.9	2.458
BB2	200 × 200	321.4	141.9	2.266
BB7	200 × 200	345.9	141.9	2.438
BB19	115 × 150	317.8	121.6	2.613
FAT1S1	115 × 150	347.8	124.4	2.795
FAT7S1	115 × 150	393.7	127.4	3.091

Table 6. Determination of safety factor for deck of Van Brienenoord Bridge

Test number	V_{exp} (kN)	V_{BB} (kN)	$V_{BB,d}$ (kN)	V_{Ed} (kN)	$V_{BB,d}/V_{Ed}$
BB1	348.7	1162.3	721.9	236.0	3.06
BB2	321.4	1071.3	665.4	236.0	2.82
BB7	345.9	1153.0	716.1	236.0	3.03
BB19	317.8	1059.3	658.0	232.0	2.84
FAT1S1	347.8	1159.3	720.1	232.0	3.10
FAT7S1	393.7	1312.3	815.1	232.0	3.51

3.4. Assessment of case study bridge for fatigue

The results of the experiments and the developed Wöhler curve can be interpreted for the assessment for fatigue. Given the geometry of the deck (see **Figure 1**), only two wheels (one of each axle) out of four wheels of the tandem can act on the deck together. The clear span is 2.1 m while the width of the design tandem is 2.4 m in total and 2.0 m center-to-center. For the interpretation of the test results, this means that the outcome of the tests with a double wheel print (Wöhler curve in **Figure 6**b) should be evaluated for the case study bridge for 250 million cycles, and that the outcome of the tests with a single wheel print (Wöhler curve in **Figure 6**b) should be evaluated for the case study bridge for 2 × 250 million cycles = 500 million cycles.

To use the Wöhler curves derived in the experiments for the assessment of the Van Brienenoord Bridge for fatigue, we will scale the fatigue load model to the 1:2 size of the test setup. Note that this approach differs from the assessment for punching, where we scaled up the capacity from the laboratory setup to the capacity of the case study bridge. Here, we use the opposite approach, to avoid having to change the Wöhler curve. The concentrated load of the fatigue load model is 105 kN. Scaling this load down to the 1:2 scale model uses a factor $2^2 = 4$, so that the concentrated load becomes

 doi:10.20944/preprints201904.0304.v1

26.25 kN. The distributed lane load of the fatigue load model is 3.105 kN/m². For the 1:2 scale model, the distributed lane load becomes 0.776 kN/m².

In the 1:2 scale model, only concentrated loads are used, so the load that represents the concentrated load as well as the distributed lane load should be determined. To determine the region over which the distributed lane load should be considered, the cracking patterns in the experiments were studied. The cracking pattern extends over 1.2 m for the experiments with a single wheel load and over 2 m for the experiments with a double wheel load. To find the equivalent point load, we determine first the bending moment caused by the distributed load, considering that the slab spans over 1.8 m:

$$M_{dist,1wheel} = \frac{1}{8}\left(0.776\frac{\text{kN}}{\text{m}^2}\times 1.2\text{m}\right)(1.8\text{m})^2 = 0.38\text{kNm} \tag{22}$$

$$M_{dist,2wheel} = \frac{1}{8}\left(0.776\frac{\text{kN}}{\text{m}^2}\times 2\text{m}\right)(1.8\text{m})^2 = 0.63\text{kNm} \tag{23}$$

The equivalent concentrated load is then:

$$F_{eq} = \frac{4M_{dist}}{l_{span}} \tag{24}$$

which results in F_{eq} = 0.83 kN for a single wheel load and F_{eq} = 1.40 kN for a double wheel load. The total load is then F = 27.08 kN for a single wheel load and F = 27.65 kN for a double wheel load.

The punching shear capacity of setup 2 is given in **Table 5** for FAT1S1 or cast 1 of the concrete as 124.4 kN and for FAT7S1 or cast 2 as 127.4 kN according to the Eurocode punching provisions. Recall that the design value of the enhancement factor is B_{Rd} = 1.622. As such, the design capacity of the punching resistance with the punching perimeter around one wheel load, including the enhancing effect of compressive membrane action becomes 1.622 × 124.4 kN = 201.8 kN for the most critical case (lowest capacity $V_{Rd,c}$ as a result of the lowest concrete compressive strength). To determine the capacity for punching with the case of a double wheel print, one could expect the double capacity. However, the results in **Table 2** show that the capacity in the FAT8S2 is 1.64 times the capacity in FAT7S1. This ratio is used for determining the punching shear capacity. The capacity is now 1.64 × 201.8 kN = 331.0 kN.

The load ratio can now be determined. For a single wheel load the load ratio is 27.08 kN / 201.8 kN = 0.134 and for a double wheel load the load ratio is 2 × 27.65 kN / 331.0 kN = 0.167.

For the evaluation for one wheel load, Eq. (3) is used with N = 500 million cycles. The resulting ratio is then S_{char} = 0.348. For two wheel loads, using Eq. (5) with N = 250 million cycles gives S_{char} = 0.447. The outcome of the assessment is that the margin of safety for one wheel print is 0.348 / 0.134 = 2.60 or that inversely the UC = 0.39. For the case with two wheel prints, the margin of safety is 0.447 / 0.167 = 2.68 or inversely UC = 0.37. The results for one and two wheel prints are thus very similar. The conclusion of the assessment is that based on the experimental results, we find that the case study bridge fulfils the code requirements for fatigue.

4. Discussion

In the previous two paragraphs, we calculated the Unity Checks for static punching (UC = 0.31), for fatigue punching of one wheel load after 500 million cycles of the single load (UC = 0.391), and for fatigue punching of two wheel loads after 250 million cycles of the axle (UC = 0.37). Comparing these Unity Checks leads to the conclusion that the most critical case is punching fatigue for a single wheel load. The difference between the punching fatigue Unity Check for one and two wheel loads is however negligible. In addition, the Unity Checks are small, and significantly smaller than the limiting value of 1.0. This analysis shows the beneficial effect of taking into account compressive membrane action.

All resulting Unity Checks are smaller than the limiting value of 1.0. This result means that the code requirements for static and fatigue punching are met for the case study bridge. This outcome directly shows the benefit of testing a scaled version of the Van Brienenoord Bridge in the laboratory.

In addition to the conclusion that the Van Brienenoord Bridge fulfills the code requirements for static and fatigue punching, we need to recall that this case study bridge was selected since it has the most critical geometry (largest span to depth ratio for the slab) of the existing slab-between-girder bridges in the Netherlands. As such, the conclusion becomes that all slab-between-girder bridges in the Netherlands, which form a well-defined subset of bridges in the Dutch bridge stock, fulfil the Eurocode requirements. Drawing this conclusion is valid, since these bridges were all built in the same time period, with the same materials, and same execution techniques – and are thus all very similar, with only small variations in the geometry and material properties.

One side note that we should place with the conclusion that all slab-between-girder bridges in the Netherlands fulfil the requirements for static and fatigue punching is that this conclusion is only valid for bridges without material degradation or other forms of damage. To ensure this premise, routine inspections remain necessary. Inspections are an important tool within the bridge management toolbox. When during an inspection indications of material degradation or damage are found, the bridge requires further analysis, and it should be evaluated if the conclusion that was based on an undamaged structure is still valid.

For this research, the outcome is twofold: 1) the small resulting Unity Checks based on the experimental results, and 2) the fact that with this approach the existing slab-between-girder bridges have been shown to fulfil the code requirements. This result also shows that constructing the 1:2 scale setups in the laboratory has been beneficial for the assessment of existing slab-between-girder bridges. While building a 1:2 scale bridge in the laboratory may be considered expensive and time-consuming, testing such a setup gives unique insights in the overall structural behavior of a structural system. Testing at the component level cannot provide such insights. Therefore, the cost-benefit analysis of these experiments is in favor of testing a structural system. Taking this approach is not common, but may be become an interesting approach for ministries or departments of transportation when they are confronted with a problem for an entire category of bridges.

5. Conclusions

A number of existing slab-between-girder bridges in the Netherlands do not fulfil the requirements of the newly introduced Eurocodes when these are evaluated for punching (both static and for cycles of loading). The Eurocode model for determining the punching shear capacity is an empirical model, derived from the results of (mostly concentric) slab-column connection tests [40]. The structural behavior of the thin slabs in slab-between-girder bridges is different from that of slab-column connections. In particular, the development of compressive membrane action increases the capacity significantly.

To study the structural behavior of slab-between-girder bridges, we selected as a case study the Van Brienenoord Bridge because it has the most critical slab geometry (largest span-to-depth ratio for the slabs) of this subset of bridges in the Dutch bridge stock. Based on the geometry of the case study bridge, we built two setups in the laboratory at 1:2 scale and carried out static and dynamic tests.

The outcome of the static tests can be used for assessing the static punching strength of the Van Brienenoord Bridge. Using the method given in the Eurocode for design by testing, a factor for converting mean values in design values of 1.53 is derived. Using this approach, the resulting Unity Check for punching shear of the Van Brienenoord Bridge becomes 0.31.

The outcome of the fatigue tests can be used to derive the Wöhler curve for thin slabs in slab-between-girder bridges. Analyzing the fatigue live load model, we select two critical loading cases for the fatigue assessment: the case with a single wheel load, and the case with two wheel loads (one of each axle). For both cases, we have the results of fatigue tests, and thus a Wöhler curve. The assessment is then carried out based on a service life of 100 years, which leads to 500 million cycles for the single wheel load and 250 million cycles for the double wheel load. Taking into account the factor to convert mean values to design values of 1.622 as derived from the static tests, we can then compare the applied load ratio to the load ratio resulting from the characteristic (5% lower bound)

 doi:10.20944/preprints201904.0304.v1

Wöhler curve. Comparing these values gives a Unity Check of 0.39 for the case with a single wheel print and of 0.37 for the case with a double wheel print.

Evaluating the results of the Unity Checks, we can identify the most critical case, which is (by a small margin) the case of fatigue punching under a single wheel load. The resulting Unity Checks are however much smaller than the limiting value of 1.0. As such, the conclusion is that the Van Brienenoord Bridge fulfils the Eurocode requirements for static punching and fatigue. Since the case study bridge is selected based on the most critical geometry, we can say that by extent all other slab-between-girder bridges in the Netherlands fulfil the Eurocode requirements for static and fatigue punching. This final conclusion, however, is only valid for bridges without deterioration and material degradation. Routine inspections remain an important bridge management tool to identify bridges that require further study.

List of notations

b	width
c	concrete cover
d	average effective depth
d_l	effective depth to the longitudinal reinforcement
d_t	effective depth to the transverse reinforcement
$f_{ck,cube}$	characteristic cube concrete compressive strength
$f_{cm,cube}$	average cube concrete compressive strength
f_{ck}	characteristic cylinder concrete compressive strength
f_{cm}	average cylinder concrete compressive strength
h	height
k	size effect factor
k_1	factor on effect of axial stresses
l	length
l_{span}	span length
q_{ik}	distributed lane load
u	punching perimeter length
v_{min}	lower bound of shear capacity
$v_{R,c}$	mean capacity for punching shear
$v_{Rd,c}$	design capacity for punching shear
$A_{s,l}$	longitudinal reinforcement area
A_{sp}	area of prestressing steel
$A_{s,t}$	transverse reinforcement area
A_u	area within punching perimeter
B_{Rd}	design capacity derived from statistical results of experiments
COV	coefficient of variation
$C_{Rd,c}$	constant in punching capacity equation
DL	dead load
DW	superimposed dead load
F	applied load
F_{eq}	equivalent load
LL	live load
$M_{dist,1wheel}$	bending moment caused by distributed lane load for influence area of one wheel load
$M_{dist,2wheel}$	bending moment caused by distributed lane load for influence area of two wheel loads
N	number of cycles
P_{max}	load at failure
Q_{ik}	axle load of design tandem
S	load ratio
S_{char}	characteristic value of load ratio (5% lower bound Wöhler curve)
U	load combination

UC Unity Check
V_{BB} average capacity of deck of Van Brienenoord Bridge based on experiments
$V_{BB,d}$ design capacity of deck of Van Brienenoord Bridge based on experiments
$V_{R,c}$ mean value of the punching shear capacity
$V_{Rd,c}$ design value of the punching shear capacity
V_{Ed} design value of punching shear demand
V_{exp} experimental punching capacity
α factor that considered effect of experiments
α_{qi} factor on distributed lane loads
α_{Qi} factor on design tandem
β reliability index
γ_T partial factor derived from experiments
μ mean value of experimental results
ρ_{avg} average reinforcement ratio
ρ_l longitudinal reinforcement ratio
ρ_t transverse reinforcement ratio
σ_{cp} average axial stress
σ_{cx} longitudinal axial stress
σ_{cy} transverse axial stress

Author Contributions: conceptualization, CV and HS; methodology, CV, RK and EL; validation, EL; formal analysis, RK and EL; investigation, RK and CV; resources, HS; data curation, EL and RK; writing—original draft preparation, EL; writing—review and editing, RK, CV and HS; visualization, RK and EL; supervision, CV and HS; project administration, CV and HS; funding acquisition, CV.

Funding: This research was funded by Rijkswaterstaat, Ministry of Infrastructure and the Environment. The APC was funded by Delft University of Technology.

Acknowledgments: The authors wish to express their gratitude and sincere appreciation to the Dutch Ministry of Infrastructure and the Environment (Rijkswaterstaat) for financing this research work. We are deeply indebted to our colleague Albert Bosman for his work in the laboratory and the meticulous reporting of the first series of experiments. We'd also like to thank our former colleagues Sana Amir and Patrick van Hemert for their contributions to the beginning of the experimental work.

Conflicts of Interest: The authors declare no conflict of interest. The funders had no role in the design of the study; in the collection and analyses of data. The funders were involved with the practical interpretation of the data, writing of the manuscript, and decision to publish the results.

References

1. CEN. Eurocode 1: Actions on structures - Part 2: Traffic loads on bridges, NEN-EN 1991-2:2003. Comité Européen de Normalisation: Brussels, Belgium, 2003; p 168.
2. Code Committee 351001. *NEN 6720 Technical Foundations for Building Codes, Concrete provisions TGB 1990 - Structural requirements and calculation methods (VBC 1995) (in Dutch)*; Civil engineering center for research and regulation, Dutch Normalization Institute,: Delft, The Netherlands, 1995; pp. 245.
3. CEN. Eurocode 2: Design of Concrete Structures - Part 1-1 General Rules and Rules for Buildings. NEN-EN 1992-1-1:2005. Comité Européen de Normalisation: Brussels, Belgium, 2005; p 229.
4. Lantsoght, E.O.L.; van der Veen, C.; de Boer, A.; Walraven, J.C. Recommendations for the Shear Assessment of Reinforced Concrete Slab Bridges from Experiments *Structural Engineering International* **2013**, *23*, 418-426.
5. Amir, S.; Van der Veen , C.; Walraven, J.C.; de Boer, A. Experiments on Punching Shear Behavior of Prestressed Concrete Bridge Decks. *Aci Structural Journal* **2016**, *113*, 627-636.
6. Teworte, F.; Herbrand, M.; Hegger, J. Structural Assessment of Concrete Bridges in Germany — Shear Resistance under Static and Fatigue Loading. *Structural Engineering International* **2015**, *25*, 266-274.
7. Bagge, N.; Nilimaa, J.; Puurula, A.; Täljsten, B.; Blanksvärd, T.; Sas, G.; Elfgren, L.; Carolin, A. Full-Scale Tests to Failure Compared to Assessments – Three Concrete Bridges. In Proceedings of fib symposium 2017, Maastricht, the Netherlands.
8. Brühwiler, E.; Vogel, T.; Lang, T.; Luechinger, P. Swiss Standards for Existing Structures. *Structural Engineering International* **2012**, *22*, 275-280, doi:10.2749/101686612x13291382991209.

9. Kong, J.S.; Frangopol, D.M. Probabilistic optimization of aging structures considering maintenance and failure costs. *Journal of Structural Engineering-Asce* **2005**, *131*, 600-616, doi:10.1061/(asce)0733-9445(2005)131:4(600).

10. Frangopol, D.M.; Sabatino, S.; Dong, Y. Bridge Life-Cycle Performance and Cost: Analysis, Prediction, Optimization and Decision Making. In Proceedings of Maintenance, Monitoring, Safety, Risk and Resilience of Bridges and Bridge Networks, Foz do Iguacu, Brazil; pp. 2-20.

11. Vergoossen, R.; Naaktgeboren, M.; 't Hart, M.; De Boer, A.; Van Vugt, E. Quick Scan on Shear in Existing Slab Type Viaducts. In Proceedings of International IABSE Conference, Assessment, Upgrading and Refurbishment of Infrastructures, Rotterdam, The Netherlands; p. 8.

12. Lantsoght, E.O.L.; van der Veen, C.; de Boer, A.; Walraven, J. Using Eurocodes and AASHTO for assessing shear in slab bridges. *Proceedings of the Institution of Civil Engineers – Bridge Engineering* **2016**, *169*, 285-297.

13. Amir, S. Compressive Membrane Action in Prestressed Concrete Deck Slabs. PhD Thesis. Delft University of Technology, 2014.

14. Collings, D.; Sagaseta, J. A review of arching and compressive membrane action in concrete bridges. *Institution of Civil Engineers – Bridge Engineering* **2015**, *169*, 271-284.

15. Eyre, J.R. Direct assessment of safe strengths of RC slabs under membrane action. *Journal of Structural Engineering-Asce* **1997**, *123*, 1331-1338.

16. Highways Agency. *Corrections within design manual for roads and bridges, use of compressive membrane action in bridge decks*; London, United Kingdom, 2007; pp 35-51.

17. Kirkpatrick, J.; Rankin, G.I.B.; Long, A.E. The influence of compressive membrane action on the serviceability of beam and slab bridge decks. *The structural engineer* **1986**, *64B*, 6-9.

18. Kuang, J.S.; Morley, C.T. A Plasticity Model for Punching Shear of Laterally Restrained Slabs with Compressive Membrane Action. *International Journal of Mechanical Sciences* **1993**, *35*, 371-385.

19. Tong, P.Y.; de V. Batchelor, B. Compressive membrane enhancement in two-way bridge slabs. *SP 30-12* **1972**, 271-286.

20. Hewitt, B.E.; de Batchelor, B.V. Punching shear strenght of restrained slabs. *Journal of the Structural Division* **1975**, *101*, 1837-1853.

21. Lantsoght, E.O.L.; Van der Veen , C.; R.T. Koekkoek; Sliedrecht, H. Capacity of prestressed concrete bridge decks under fatigue loading. In Proceedings of fib symposium 2019, Cracow, Poland.

22. Bennett, E.W.; Muir, S.E.S.J. Some fatigue tests of high-strength concrete in axial compression. *Magazine of Concrete Research* **1967**, *19*, 113-117.

23. Lantsoght, E.O.L.; van der Veen, C.; de Boer, A. Proposal for the fatigue strength of concrete under cycles of compression. *Construction and Building Materials* **2016**, *107*, 138-156.

24. Isojeh, B.; El-Zeghayar, M.; Vecchio, F.J. Fatigue Resistance of Steel Fiber-Reinforced Concrete Deep Beams. *ACI Structural Journal* **2017**, *114*, doi:10.14359/51700792.

25. Teng, S.; Ma, W.; Tan, K.H.; Kong, F.K. Fatigue tests of reinforced concrete deep beams. *The structural engineer* **1998**, *76*, 347-352.

26. Teworte, F.; Hegger, J. Shear Fatigue of Prestressed Concrete Beams. In Proceedings of IABSE 2011; p. 8.

27. Muller, J.F.; Dux, P.F. Fatigue of Prestressed Concrete Beams with Inclined Strands. *Journal of Structural Engineering* **1994**, *120*, 1122-1139, doi:doi:10.1061/(ASCE)0733-9445(1994)120:4(1122).

28. Yuan, M.; Yan, D.; Zhong, H.; Liu, Y. Experimental investigation of high-cycle fatigue behavior for prestressed concrete box-girders. *Construction and Building Materials* **2017**, *157*, 424-437, doi:https://doi.org/10.1016/j.conbuildmat.2017.09.131.

29. Fujiyama, C.; Gebreyouhannes, E.; Maekawa, K. Present Achievement and Future Possibility of Fatigue Life Simulation Technology for RC Bridge Deck Slabs. *Society for Social Management Systems Internet Journal* **2008**, *4*.

30. Harajli, M.H.; Naaman, A.E. Static and Fatigue Tests on Partially Prestressed Beams. *Journal of Structural Engineering* **1985**, *111*, 1602-1618, doi:doi:10.1061/(ASCE)0733-9445(1985)111:7(1602).

31. Xin, Q.; Dou, Y.; Chen, W. *Load Spectrum and Fatigue Life Computer Analysis of Prestressed Concrete Bridges*; 2015; Vol. 9, pp. 247-266.

32. Rijkswaterstaat. Guidelines Assessment Bridges - assessment of structural safety of an existing bridge at reconstruction, usage and disapproval (in Dutch), RTD 1006:2013 1.1. Utrecht, the Netherlands, 2013; p 117.

33. Van der Veen , C.; Bosman, A. *Vermoeiingssterkte voorgespannen tussenstort*; Stevin Report nr. 25.5-14-06, Delft University of Technology, Delft, the Netherlands. 2014; p 65.

34. Lantsoght, E.O.L.; Van der Veen , C.; Koekkoek, R.T.; Sliedrecht, H. Fatigue testing of transversely prestressed concrete decks. *ACI Structural Journal* **in press**.

35. Koekkoek, R.T.; van der Veen, C.; de Boer, A. Fatigue Tests on Post-tensioned Bridge Decks. fib Symposium 2017, Maastricht, the Netherlands; pp. 912-920.

36. Koekkoek, R.T.; van der Veen, C. *Measurement Report Fatigue Tests on Slabs Cast In-Between Prestressed Concrete Beams*; Stevin Report nr. 25.5-17-14, Delft University of Technology, Delft, the Netherlands. 2017; p 196.
37. Lantsoght, E.O.L.; Van der Veen , C.; Koekkoek, R.T.; Sliedrecht, H. Punching capacity of prestressed concrete bridge decks under fatigue. *ACI Structural Journal* **in press**.
38. Code Committee 351001. *Assessement of structural safety of an existing structure at repair or unfit for use - Basic Requirements, NEN 8700:2011 (in Dutch)*; Civil center for the execution of research and standard, Dutch Normalisation Institute: Delft, The Netherlands, 2011; pp. 56.
39. CEN. Eurocode – Basis of structural design, NEN-EN 1990:2002 Comité Européen de Normalisation: Brussels, Belgium, 2002; p 103.
40. Walraven, J.C. *Background document for EC-2, Chapter 6.4 Punching Shear*; Stevin Report Nr. 25.5-02-37. Delft University of Technology: Delft, The Netherlands, 2002; pp 1-16.